INVITED PAPER *Special Section on Electronic Displays*

An Advanced 405-nm Laser Diode Crystallization Method of a-Si Film for Fabricating Microcrystalline-Si TFTs

Kiyoshi MORIMOTO[†a)], **Nobuyasu SUZUKI**[†], **Kazuhiko YAMANAKA**[†], **Masaaki YURI**[†], **Janet MILLIEZ**[††], ***and*** **Xinbing LIU**[†††], ***Nonmembers***

SUMMARY This report describes a crystallization method we developed for amorphous (a)-Si film by using 405-nm laser diodes (LDs). The proposed method has been used to fabricate bottom gate (BG) microcrystalline (μc)-Si TFTs for the first time. A μc-Si film with high crystallinity was produced and high-performance BG μc-Si TFTs with a field effect mobility of 3.6 cm^2/Vs and a current on/off ratio exceeding 10^8 were successfully demonstrated. To determine the advantages of a 405-nm wavelength, a heat flow simulation was performed with full consideration of light interference effects. Among commercially available solid-state lasers and LDs with wavelengths having relatively high optical absorption coefficients for a-Si, three (405, 445, and 532 nm) were used in the simulation for comparison. Results demonstrated that wavelength is a crucial factor for the uniformity, efficiency, and process margin in a-Si crystallization for BG μc-Si TFTs. The 405-nm wavelength had the best simulation results. In addition, the maximum temperature profile on the gate electrode through the simulation well explained the actual crystallinity distributions of the μc-Si films.

key words: *laser crystallization of a-Si, thin film transistor, microcrystalline silicon, heat flow simulation*

1. Introduction

High field-effect mobility and electrical stability on backplane TFTs are strongly desired for future active-matrix OLEDs and LCDs, as is a reduction to the cost of production. Bottom gate (BG) microcrystalline (μc)-Si TFTs are promising candidates to meet the above requirements: they are inexpensive and have good scalability to large-sized glass substrates because the device structure and process are almost identical to those of amorphous (a)-Si:H TFTs except that they require an additional process of a-Si crystallization. Laser crystallization with visible lasers such as 405-nm laser diodes (LDs) [1], 445-nm LDs [2], and 532-nm Nd:YAG (SHG) lasers [3] have attracted much attention recently due to their longer maintenance cycle, lower equipment cost, and more stable beam intensity than ultra-violet excimer lasers. The visible laser crystallization of a-Si for BG μc-Si TFTs fabrication is therefore considered to have huge potential, although only a few have been reported so far [4], [5]. In this work, we propose a 405-nm LD crystallization method of a-Si for BG μc-Si TFTs and investigate its validity through TFT fabrication and heat flow simulation.

Manuscript received February 22, 2011.
Manuscript revised June 6, 2011.

[†]The authors are with Panasonic Corporation, Kadoma-shi, 571-8501 Japan.
[††]The author was with Panasonic Corporation of North America, Secaucus, New Jersey 07094, USA, and currently with Osram Sylvania, Danvers, MA 01923, USA.
[†††]The author is with Panasonic Corporation of North America, Secaucus, New Jersey 07094, USA.
a) E-mail: morimoto.kiyoshi@jp.panasonic.com
DOI: 10.1587/transele.E94.C.1733

2. Experimental Methods

Figure 1 shows the wavelength dependence of the optical absorption coefficient α for a-Si and poly-Si. Due to a larger α for a-Si at 405 nm than those at 445 and 532 nm, we expect more efficient crystallization of a-Si. The large difference between a-Si and poly-Si at 405 nm enables the selective heating of a-Si. In addition, the 405-nm LDs can provide stable, simple, low-energy a-Si crystallization because of the inherent LD characteristics.

Figure 2 shows a schematic of the device used in the crystallization process. A 120-nm-thick SiN film was formed on a 0.7-mm-thick glass substrate for the impurity diffusion prevention and thermal isolation between the substrate and the device active area during laser crystallization. The SiN film was deposited by radio-frequency (RF) plasma-enhanced chemical vapor deposition (PECVD). Then, a gate electrode of a high melting point metal such as Molybdenum was formed on the SiN film by sputtering and the gate electrode was patterned by conventional lithography and dry etching. The nominal width and thickness of the gate pattern was 30 μm and 50 nm, respectively. In addition, a 120-nm-thick SiO_2 as gate insulator was deposited by RF-PECVD. Next, as precursor, a 35-nm-thick hydrogenated a-Si film was deposited on the gate in-

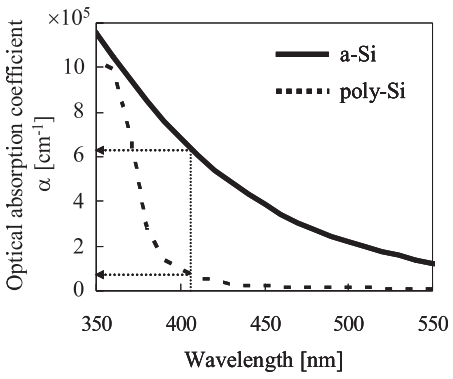

Fig. 1 Wavelength dependence of the optical absorption coefficient for a- Si and poly-Si.

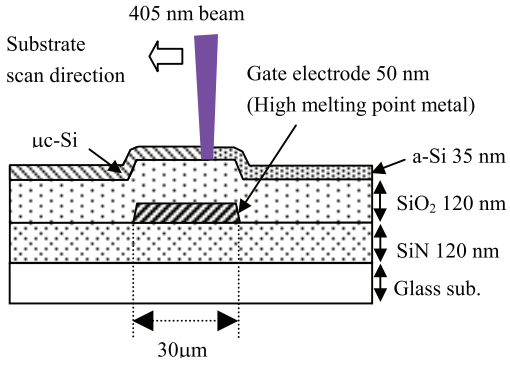

Fig. 2 Cross-sectional view of the device.

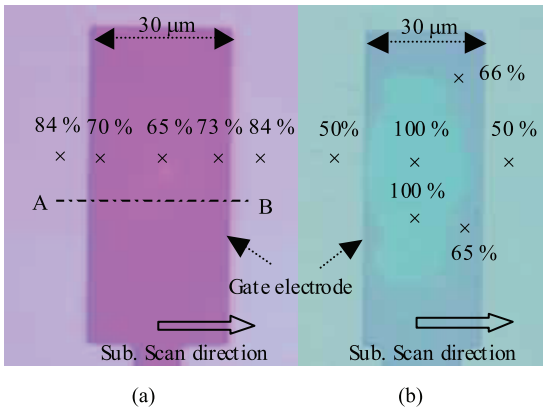

Fig. 3 Optical microscope images of the μc-Si crystallized by (a) 405- and (b) 532-nm beams.

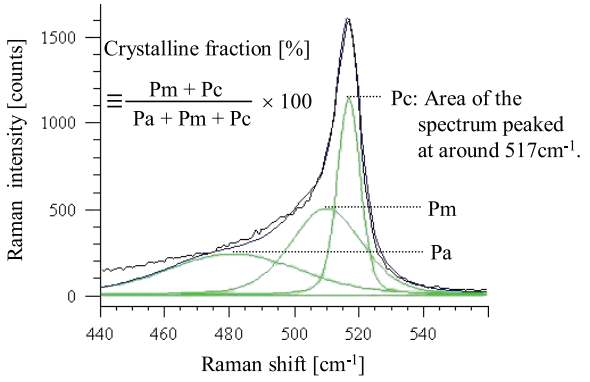

Fig. 4 Raman spectrum of the μc-Si film with a crystalline fraction of 65%.

sulator by RF-PECVD and was dehydrated above 450°C in nitrogen gas ambient.

A flat-top shaped beam was obtained by combining 405-nm LDs and optics consisting of a collimator, aspheric, and condenser lenses. The beam profile was 5–30 μm at FWHM (short axis, scan direction) × 30–200 μm at a light intensity of 90% (long axis, perpendicular to the short one, variable by changing the LDs and the aspheric lens). The profile along the short axis had a Gaussian-like distribution and the peak to peak variation of the beam intensity along the long axis was within 5% with optimized optics.

A glass substrate with the device shown in Fig. 2 was set on the motor-driven x-y planar motion stage and the 405-nm LD crystallization of the a-Si was performed in air with adequate LD power and scan speed of the stage. The maximum power density and scan speed in this experiment were 70 kW/cm^2 and 150 mm/s, respectively. Typical conditions for μc-Si formation were 23.5 kW/cm^2 and 40 mm/s. The TFT fabrication was based on a conventional process for back-etch type BG TFTs. After the laser crystallization, the μc-Si film was exposed to hydrogen plasma to reduce crystalline defects induced during the laser scan. Next, a second a-Si film was deposited by RF-PECVD and the channel area was patterned. An n$^+$-contact a-Si film was then deposited by RF-PECVD, followed by electrode metal deposition by sputtering. Then the metal layer was patterned by wet chemical etching through a photo resist mask and the n$^+$-contact a-Si layer was sequentially patterned by dry etching through the same mask. Finally a SiN passivation film was deposited.

The crystallized Si films were characterized by a scanning electron microscope (SEM, Hitachi S-4500) and micro-Raman scattering spectroscopy system (Tokyo Instruments Nanofinder-30). Electrical characteristics of the BG μc-Si TFTs were evaluated with the Keithley 236 source-measurement unit.

3. Results

3.1 μc-Si Film Properties

Figure 3(a) shows an optical microscope image of the μc-Si crystallized by a 405-nm beam. Figure 3(b) shows an image by a 532-nm flat-top beam for comparison. Crystalline fractions at several points are indicated in both images. The fraction was calculated from the areal ratio of the three decomposed peaks at around 480 (Pa: a-Si), 510 (Pm: μc-Si), and 517 (Pc: poly-Si) cm^{-1}, as shown in Fig. 4. In Fig. 3(a), the fraction of μc-Si above the gate is lower than that above SiO_2 (non-gate region), whereas in Fig. 3(b), it behaves inversely. Furthermore, in both images, the 405-nm crystallization exhibited more uniform crystallinity of μc-Si above the gate than that by 532-nm. These results will be discussed in more detail in Sect. 4.

To evaluate the crystallinity profile of μc-Si by 405 nm, we performed a one-dimensional Raman measurement along the line from A to B in Fig. 3(a). The in-plane spatial resolution was approximately 0.3 μm under 488 nm excitation. Figure 5 shows the results. In the channel region, the crystalline fraction is constant at 65%. This value increases gradually as the distance from the gate increases. The crystalline fraction of 65% corresponds to a grain size 20–30 nm in diameter, which was confirmed by SEM observation after Secco etching (Fig. 6). The profile in Fig. 5 is ideal for TFT applications because of the increased crystallinity of μc-Si at the drain/source contacts, which leads to better device char-

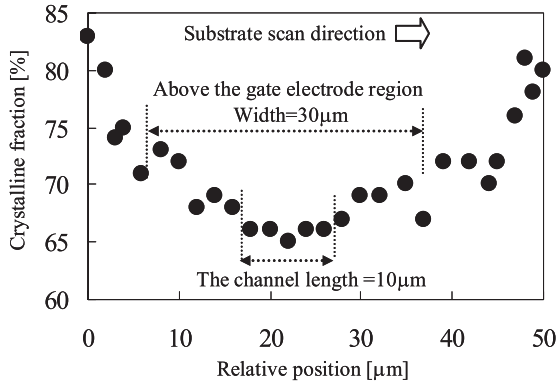

Fig. 5 Crystalline fraction profile of the μc-Si film along the gate electrode (line – · – · – from A to B in Fig. 4(a)).

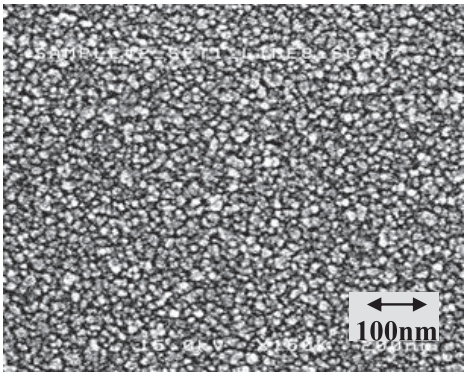

Fig. 6 SEM image of the Secco-etched μc-Si film with a crystalline fraction of 65%.

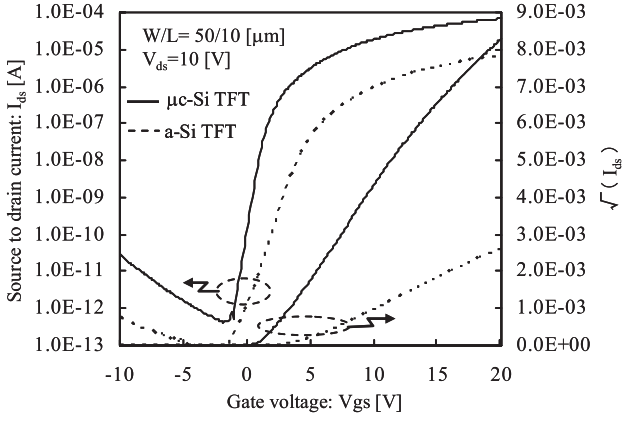

Fig. 7 Typical transfer curves of the BG μc-Si TFTs by the proposed method.

acteristics including low contact resistance and off-current.

3.2 Electrical Characteristics of TFTs

Figure 7 shows the transfer curves of a-Si and μc-Si TFTs fabricated on the same substrate. The nominal channel width and length of these TFTs are 50 and 10 μm, respectively. A drain-source voltage V_{ds} of 10 V was applied. The TFT parameters were extracted from the electrical characteristics shown in Fig. 7 and are summarized in Table 1.

Table 1 Extracted TFT parameters.

TFT parameters \ Channel type	a-Si	μc-Si
Threshold voltage: Vt [V]	4.4	1.5
Field effect mobility: μ [cm^2/Vs]	0.4	3.6
Current on/off ratio	1.1×10^8	1.6×10^8
Subthreshold slope: S [V/dec]	0.91	0.47
Vt shift: ΔVt [V]	1.6	0.06

Concerning the reliability of the TFTs, we investigated their electrical stability under bias stress, with V_{ds} set to 11.5 V and the gate-source voltage V_{gs} set to the threshold voltage Vt plus 5 V. After a stress time of 2×10^5 sec at room temperature, the Vt shift ΔVt for the BG μc-Si TFTs was 0.06 V, which is much smaller than the 1.6 V shift in the a-Si TFTs. The obtained values of the Vt shift are also listed in Table 1. These values clearly show that the μc-Si TFT has superior parameters compared to those of the a-Si TFT. In addition, our μc-Si TFTs have higher μ, steeper S, and lower Vt than those in previous studies [4], [6], although the current on/off ratio is comparable. These excellent BG μc-Si TFT characteristics are considered the result of high crystallinity in the channel region and good source/drain contacts (as previously stated in Sect. 3.1).

4. Discussion

In order to evaluate the validity of 405 nm, we performed a two-dimensional heat flow simulation based on Eq. (1) by using a finite element method. The device structure for the simulation is identical to that in Fig. 2.

$$\frac{\partial T(x,y)}{\partial t} = \frac{\kappa}{\rho C_p}\left(\frac{\partial^2 T(x,y)}{\partial x^2} + \frac{\partial^2 T(x,y)}{\partial y^2}\right) + \frac{S}{\rho C_p} \qquad (1)$$

Here, x is the position along the laser beam scanning direction, y is the depth from the surface of the a-Si film, T is the temperature, t is the time, κ, ρ, and C_p are the thermal conductivity, density, and specific heat, respectively, and S is the generated heat energy by laser absorption. We can roughly estimate the optical absorptance of the a-Si by using the simple formula $(1 - R)(1 - e^{-d\alpha})$, where R and d are the reflectance and the thickness, respectively, of a-Si. However, in this work we calculated the absorptance by fully considering the optical interference effect [7] among the multi-layers of the device structure shown in Fig. 2. The absorptance of the a-Si above the gate electrode or only SiO_2 (non-gate region) was calculated based on the layered structures in Figs. 8(a) and (b), respectively. Complex refractive index and thickness of each layer are needed to calculate the optical absorptance of the a-Si in Fig. 8. We used the optical constants in Table 2 in order to perform the heat flow simulation at three wavelengths of 405, 445, and 532 nm for comparison.

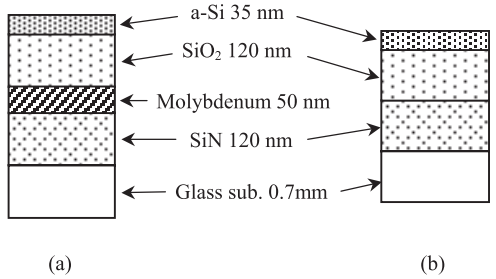

Fig. 8 Layered structures used in the absorptance calculation of the a-Si above (a) the gate electrode and (b) only SiO_2 (non-gate region).

Table 2 Optical constants of the materials in the absorptance calculation of the a-Si.

Materials	Complex refractive index		
	405 nm	445 nm	532 nm
a-Si	5.31+2.19 *i*	5.38+1.51 *i*	5.06+0.61 *i*
SiO_2	1.47	1.46	1.46
Molybdenum	2.88+3.46 *i*	3.04+3.68 *i*	3.47+3.78 *i*
SiN	2.07	1.98	1.90
Glass (substrate)	1.52	1.52	1.51

Table 3 Detailed conditions of the heat flow simulation.

Wavelength [nm]	405	445	532
Power density [kW/cm^2]	70		175
Beam scanning speed [mm/sec]	500		
Beam FWHM [μm]	30		
Beam scanning distance [μm]	140		

Table 4 Thermal constants of the materials in the heat flow simulation.

Materials	Thermal conductivity κ (W/m·K)	Density ρ (Kg/m^3)	Specific heat *Cp* (J/Kg·K)
a-Si	1.0	2340	1252
SiO_2	1.6	1620	745
Molybdenum	138	10280	250
SiN	1.5	2710	711
Glass (substrate)	6.2	2600	773

Detailed conditions of the heat flow simulation are listed in Table 3. A laser beam with a Gaussian profile of FWHM 30 μm was assumed and scanned over a 30-μm-wide BG electrode pattern at a speed of 500 mm/s. In Table 4, thermal constants of the materials in the heat flow simulation are listed.

Figure 9 shows the simulated maximum temperature profiles of the a-Si in Fig. 2 for the beam scans at the three wavelengths. We determined the power density of the beam under each simulation condition to have a maximum temperature of around 1300 K, where it is expected that solid

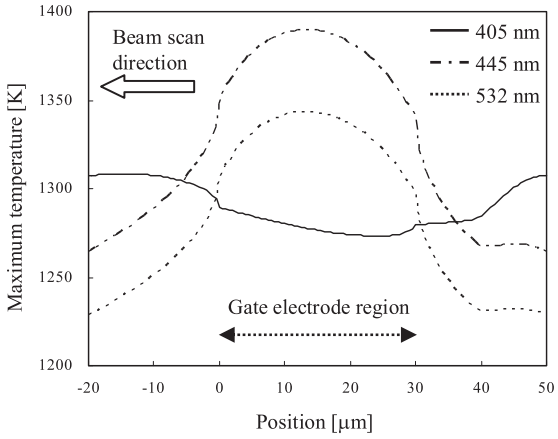

Fig. 9 Simulated maximum temperature profiles of the a-Si for the beam scans at three wavelengths.

phase crystallization of a-Si occurs in under 0.1 msec [8]. If we compare the power density at each wavelength in Table 3, the 405- and 445-nm beams produce 2.5 times more efficient heating of the a-Si than the 532-nm beam. According to Fig. 9, the 405-nm beam provides the most uniform profile of the maximum temperature above the gate electrode among the three wavelengths.

In addition, the simulation results for 405- and 532-nm agree with the crystalline fraction distributions in Figs. 3(a) and (b). Moreover, the profile for 405 nm in Fig. 9 is consistent with the profile of the crystalline fraction in Fig. 5. It should be noted that the laser beam was scanned in the heat flow simulation whereas the substrate was scanned in all the experiments instead of the beam scan. Thus the beam scan direction in Fig. 9 is opposite to the substrate scan direction in Figs. 3(a), (b), and 5.

There is only a 40-nm difference in wavelength between 405 and 445 nm, but the corresponding profiles in Fig. 9 are, interestingly, quite different in shape. In contrast, although there is a relatively large difference of 87 nm between 445 and 532 nm, the shapes of those profiles are similar. To understand these differences, let us look into the heat generation process of a-Si relating to term S in Eq. (1).

Figures 10(a) and (b) shows the relationships between the optical absorptance of the a-Si above the gate electrode or only SiO_2 (non-gate region) and the thickness of the a-Si for the three wavelengths, respectively. Here, the thickness of each layer except the a-Si layer is assumed to be the same as those shown in Figs. 8(a) and (b). Higher absorptance of the a-Si results in more efficient laser crystallization because it is converted into heat energy.

As in Fig. 10(a), only the 405-nm beam has an almost constant absorptance over the thickness change of the a-Si, which leads to the widest process window for a-Si crystallization. Figure 10(a) also reveals why the 532-nm condition needs approximately 2.5 times more power density at an a-Si thickness of 35 nm than the other two, as in Table 3 and Fig. 9. After detailed analysis of the heat flow simulation results, we found that the uniformity of the maximum

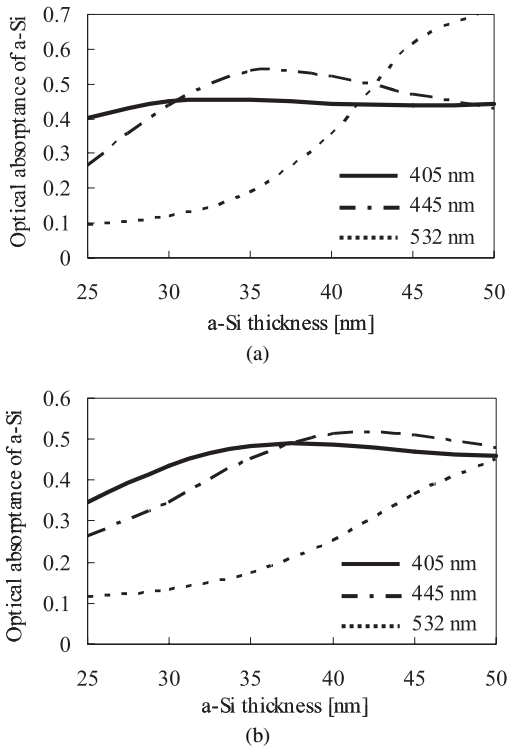

Fig. 10 Optical absorptance of the a-Si above (a) the gate and (b) non-gate region as a function of a-Si thickness.

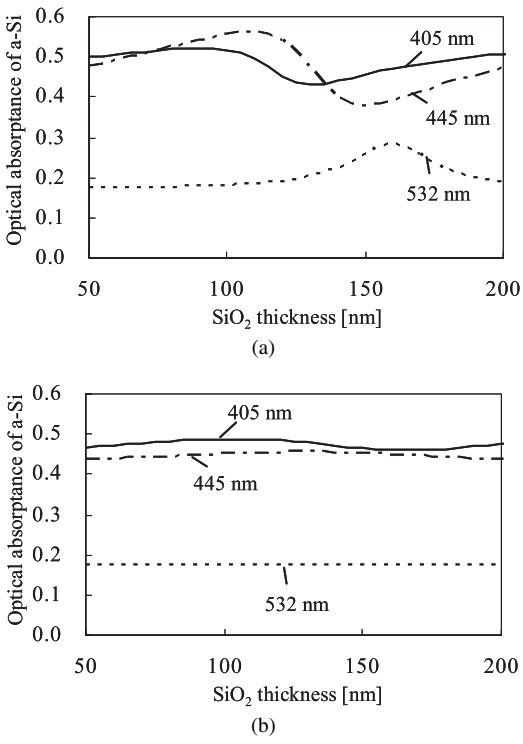

Fig. 11 Optical absorptance of the a-Si above (a) the gate and (b) non-gate region as a function of SiO_2 thickness.

temperature profiles in Fig. 9 is dominated by the difference between the optical absorptance of the a-Si above the gate and non-gate region. If we estimated the absorptance based on the simple formula $(1 - R)(1 - e^{-d\alpha})$, there would be no absorptance difference between on the gate and non-gate region and we would not be able to explain the difference of the crystalline fraction distributions in Figs. 3(a) and (b). In other words, the light interference effect plays a major role in determining the absorptance in thin a-Si thickness ranges of less than 50 nm. Therefore, thickness variations of underlying layers in Figs. 8(a) and (b), such as the SiO_2 gate insulator, should also affect the crystallization process.

Figures 11(a) and (b) show the relationships between the optical absorptance of the a-Si above the gate electrode or non-gate region and the thickness of the gate SiO_2 film for the three wavelengths, respectively. Here, the thickness of each layer except the SiO_2 layer is assumed to be the same as those shown in Figs. 8(a) and (b).

As in Fig. 11(b), the absorptance curves of a-Si on the non-gate region are relatively insensitive to variations of SiO_2 thickness in the wide range from 50 to 200 nm. In contrast, the absorptance curves on the gate region strongly depend on the SiO_2 thickness variation, as in Fig. 11(a). Comparing the three wavelengths in Fig. 11(a) shows that the relative change of the absorptance curve for 405 nm as a function of SiO_2 thickness is the smallest among the three, giving it the largest process margin.

On BG TFTs, the thickness of the a-Si is generally less than 50 nm to enable a low off-current. When visible light is used for crystallization in such a thin a-Si thickness range, the optical interference effect plays a major role in determining the light absorptance of a-Si. The wavelength of a scanned beam is therefore a crucial factor for the uniformity, efficiency, and process margin in the crystallization of a-Si. From the heat flow simulation results in Figs. 9, 10, and 11, we can conclude that the 405-nm wavelength has a tremendous advantage for a-Si crystallization of device structures commonly used in BG Si TFTs.

5. Conclusion

We proposed a method of crystallizing a-Si using 405-nm LDs and applied it to the fabrication of BG μc-Si TFTs for the first time. The TFTs were fabricated and demonstrated superior electrical characteristics. To verify this theoretically, we performed a heat flow simulation to investigate the laser wavelength dependence on uniformity and efficiency of a-Si heating for crystallization. We found that wavelength is a crucial factor in the crystallization process of thin a-Si film less than 50 nm thick. A 405-nm beam had the best results among the compared wavelengths, and it also had the widest process window against changes of the a-Si and gate insulator thickness. We believe that our 405-nm LD-based technology is a key component in fabricating high-performance BG μc-Si TFTs with inexpensive, energy-saving manufacturing, and that it has good process scalability to large-sized substrates.

Acknowledgments

The authors would like to thank Mr. Ayumu Tsujimura, Mr. Shinichi Takigawa, Dr. Tsuyoshi Tanaka, and Dr. Daisuke Ueda for continuous support, encouragement, and insightful comments. Also, the authors are indebted to Mr. Kenji Orita, Dr. Shinji Yoshida, and Dr. Katsuya Samonji for valuable discussions.

References

[1] A. Machida, T. Fujino, T. Kono, K. Takagi, S. Haga, S. Imanishi, and T. Kamei, "A poly-Si TFT fabricated by a novel laser-crystallization technique using Blu-ray disc technology," SID 09 digest, no.P-6, pp.1100–1102, San Antonio, USA, 2009.

[2] T. Noguchi, Y. Chen, T. Miyahira, J.D.D. Mugiraneza, Y. Ogino, Y. Iida, E. Sahota, and M. Terao, "Advanced micro-polycrystalline silicon films formed by blue-multi-laser-diode annealing," Jpn. J. Appl. Phys., vol.49, pp.03CA10-1-3, 2010.

[3] S. Yura, A. Sono, T. Okamoto, Y. Sato, T. Kojima, J. Nishimae, M. Inoue, and K. Motonami, "Crystallization of amorphous-Si films by pulsed YAG2ω green laser for polycrystalline Si TFT fabrication," J. SID, vol.13/10, pp.823–827, 2005.

[4] T. Okabe, T. Yaneda, T. Aita, T. Inoue, M. Takei, Y. Harumoto, H. Nishiki, and N. Kimura, "Microcrystalline silicon thin film transistors by Excimer laser annealing for large-sized TFT-LCDs," Proc. IDW'09, no.AMD2-2, pp.257–260, Miyazaki, Japan, 2009.

[5] S.H. Cho, Y.M. Cho, Y.G. Jeong, H. Kim, S.H. Yang, J.H. Song, C. Jeong, and S.Y. Kim, "New process development for hybrid silicon thin film transistor," IMID/IDMC/ASIA Display'08 Digest, no.P-3, pp.205–207, Seoul, Korea, 2008.

[6] T. Arai, N. Morosawa, Y. Inagaki, K. Tstsuki, and T. Urabe, "Micro crystalline silicon TFT by the metal capped diode laser thermal annealing method," Mater. Res. Soc. Symp. Proc., vol.1066, pp.1066-A09-02, San Francisco, USA, 2008.

[7] R.M.A. Azzam and N.M. Bashara, Ellipsometry and polarized light, chapter 4, North-Holland Personal Library, 1987.

[8] S. Higashi, H. Kaku, T. Okada, H. Murakami, and S. Miyazaki, "Crystallization of Si in millisecond time domain induced by thermal plasma JET irradiation," Jpn. J. Appl. Phys., vol.45, no.5B, pp.4313–4320, 2006.

Kiyoshi Morimoto received B.S. and M.S. degrees in Electrical Engineering from the Nagaoka University of Technology in 1986 and 1988, respectively. He has been with Panasonic since 1988, where he is engaged in the research and development of semiconductor materials and devices. From 2006–2008, he was a Visiting Scientist in the department of Materials Science and Engineering at Cornell University.

Nobuyasu Suzuki received his B.E. and M.E. degree in Electrical Engineering from the Chiba University in 1991 and 1993 respectively. He joined Panasonic Co. in 1993, where he has been engaged in research and development related to laser processing and nano-materials.

Kazuhiko Yamanaka received the B.S. and M.S. degrees in Electronic Engineering from Osaka University, Suita, Japan, in 1994 and 1996, respectively. In 1996, he joined Panasonic Corporation, Osaka, where he has been engaged in the research and development of semiconductor laser modules for optical data storage. He is now working to develop light emitting diode and laser diode with Gallium nitride based materials.

Masaaki Yuri received the B.S. and M.S. degrees in Electrical Engineering from Kyoto University, Japan, in 1985 and 1987, respectively. In 1987, he joined Panasonic Corporation, where he worked on laser diodes and light emitting diodes. During 1992–1996, he was a visiting scholar at Stanford University, working on computational analysis of lasers. He is currently responsible for development of laser diodes and wide-gap optoelectronic devices.

Janet Milliez received a Ph.D. degree in Optics from the College of Optics and Photonics/CREOL, University of Central Florida, in 2006. In 2006 she joined the Panasonic Boston Lab of Panasonic R&D Company of America as an optical engineer, where she designed novel optical systems and components for displays, material processing, and various laser applications. Since 2010 she has been an optical engineer at Osram Sylvania, Inc. where she develops LED retrofit lamps.

Xinbing Liu received a Ph.D. in Applied Physics from the University of Michigan in 1994. He has been with Panasonic Corporation of North America since 1998, and is currently director of the Panasonic Boston Laboratory in Newton, Massachusetts. He engages in R&D in laser processing and micro-optics.